




RESEARCH ARTICLE

Classification of forensic hyperspectral paper data using hybrid spectral similarity algorithms

Deepthi¹  | Binu Melit Devassy²  | Sony George²  | Peter Nussbaum² | Tessamma Thomas¹

¹Department of Electronics, Cochin University of Science and Technology, Kochi, Kerala, India

²Department of Computer Science, Norwegian University of Science and Technology, Gjøvik, Norway

Correspondence

Binu Melit Devassy, Department of Computer Science, Norwegian University of Science and Technology, Gjøvik, Norway.

Email: binu.m.devassy@ntnu.no

Abstract

Document forgeries that involve modification of the materials used, such as ink and paper, provide evidence of any malpractices being performed. Forensic specialists use different techniques to identify and classify these samples; however, the most preferred method is to use nondestructive techniques to avoid any potential damage to the original specimen under investigation. Hyperspectral imaging has already been explored in several application domains and used as a powerful method in forensic investigations to extract information about the materials under examination. To precisely classify the material information and utilize the hyperspectral imaging technique's potential, we probed the potential of some hybrid spectral similarity measures to classify different commonly used paper samples. A comparison of these methods is quantitatively presented in this article.

KEYWORDS

document forgeries, forensics, hybrid spectral similarity algorithms, hyperspectral imaging

1 | INTRODUCTION

Forgeries in the form of document fraud or counterfeiting are widely used malpractice with different objectives. In many cases, evidence from document forgeries is directly connected to the paper and ink used. Forensic experts apply various methods to analyze the paper and ink samples used in the document to investigate and trace these samples to verify their originality. Chemical analysis,^{1,2} and other destructive³ techniques, that may destroy the original specimen also require more processing time and are also limited by the region of the document it can analyze. Ultraviolet (UV) and near-infrared (NIR) imaging,⁴ as well as visual inspection, are also used very commonly in this domain. Spectral information from the document under investigation can provide valuable information about the paper and the ink used in the document. Motivated by these facts, hyperspectral imaging (HSI), which integrates spectral and spatial information, recently became one of the most potent tools in forensic investigations.

HSI combines spectroscopy, and imaging and this technique provide spectral information across the whole spatial area of the object under investigation. HSI has been used widely in different sectors like remote sensing,⁵ cultural heritage,⁶ medical imaging,⁷ food,⁸ and forensics⁹ for different purposes such as documentation, classification, material identification, and visualization. Hundreds of narrowband images recorded in the visible and near-infrared (VNIR)

This is an open access article under the terms of the Creative Commons Attribution-NonCommercial-NoDerivs License, which permits use and distribution in any medium, provided the original work is properly cited, the use is non-commercial and no modifications or adaptations are made.

© 2022 The Authors. *Journal of Chemometrics* published by John Wiley & Sons Ltd.

region of the electromagnetic spectrum open up the possibility to accurately classify the material's constituents under inspection. Once the HSI data are acquired from the questioned document, various pre-processing steps are followed before classification. Existing spectral classification algorithms¹⁰ are designed based on the distinction power of the spectral signature of materials. Generally, the accuracy of these classification algorithms determines the applicability of the HSI technique.

This study probes spectral similarity measures (SSM), supervised pattern recognition approaches that efficiently utilize spectral signatures' information to classify materials. Also, the spectral matching measures are highly effective in classifying target materials as they can mitigate illumination effects, such as gain and offset errors.¹¹ Here, the classification accuracy primarily relies upon the spectral similarity measure and the properties of the specific spectrally defined targets.¹² Technically the spectral similarity measure compares the degree of similarity between two spectra, that is, between an unknown image pixel spectrum and a reference spectrum, where the comparison is made using the similarity as a criterion.¹³ The reference spectra can be collected from laboratory or field spectra or extracted directly from the image data as a single-pixel spectrum or averages of spectra from a region of interest.^{14,15} Normally, information extraction from images is achieved by applying the individual SSM like city block distance (CBD),¹⁶ euclidean distance (EUD),¹⁷ spectral angle mapper (SAM),¹⁴ spectral correlation angle (SCA),¹⁸ spectral information divergence (SID),¹⁹ jeffries–matusita distance (JMD),²⁰ and chi-square distance (CHI).^{21,22} In this work, instead of modifying existing algorithms, hybrid SSM are explored to understand and evaluate their classification accuracy. Many studies have been conducted to evaluate the individual SSM and the necessity of hybrid ones; they revealed the limitations of the individual spectral matching methods and recommended developing hybrid measures that can overcome the limitations by integrating the benefits of individual measures.^{19,20,23–25} However, very little study has been done on the use of hybrid SSM for forensic investigations; this paper aims to investigate the performances of these measures on the forensic paper data classification using a dataset of 40 paper samples. The hybrid SSM are chosen based on spectral discriminatory measures, namely, relative spectral discriminatory probability (RSDPB),²³ relative spectral discriminatory power (RSDPW),²³ and relative spectral discriminatory entropy (RSDE).^{23,26,27} The chosen hybrid spectral similarity measures are SID-SAM,²⁸ SID-SCA,²³ SID-CBD,²⁵ SID-EUD,²⁵ CHI-SAM,²⁵ CHI-SCM, JMD-CHI,²⁵ and SID-CHI.²⁹ The outcomes of the classifications are summarized using the confusion matrices and evaluated for overall accuracy (OA),^{30–35} kappa (\hat{K}),³⁶ Z-score of kappa ($Z(\hat{K})$),³⁷ 95% confidence interval of kappa ($CI(\hat{K})$),³⁸ coefficient of determination (R^2), mean absolute error (MAE), and root mean squared error (RMSE). The results revealed the multiclass classification capability of hybrid SSM where the SID-SCA performed well on hyperspectral image data (VNIR) of paper samples compared with other SSM.

The remaining portion of this paper is organized into three parts; Section 2 will explain the sample preparation and acquisition of HSI data. The SSM are discussed in Section 3. The findings will be addressed in the following part along with the discussions, and the final section describes the conclusion and potential future works.

2 | MATERIALS AND HSI ACQUISITION

2.1 | Samples and hyperspectral image acquisition

The samples used in this study were already presented in our previous work,³⁹ which contains 40 commonly used paper types collected and arranged as a checkerboard pattern (10 rows \times 4 columns). Each sample has a square shape with 4 cm long sides, as shown in Figure 1. Hyperspectral image acquisition of the paper samples was conducted using the hyperspectral push-broom camera HySpex VNIR-1800 (Developed by Norsk Elektro Optikk AS, Norway). The sensitivity of this camera is from 400 to 1000 nm with a spectral sampling of 3.18 nm and a spatial resolution of 1800 pixels across the field of view. The acquisition configuration is the same as in the previous work,³⁹ where the chart containing different paper samples is placed perpendicular to the camera on a moving translator stage. Two halogen light sources were used to illuminate the samples with an imaging geometry of 45°:0° with respect to the camera. The camera corrections, such as dark current subtraction, sensor corrections, and radiometric calibration, were carried out by HySpex RAD, a preprocessing software provided by the camera manufacture. As a reference object, a contrast multi-step reference target with known reflectance values was used. In order to recover the reflectance of the paper samples, the known reflectance values of this reference target are used. The output HSI data cube has a resolution of 1800 \times 7500 \times 186 (width \times length \times bands) pixels and a dynamic range of 16-bit unsigned integers. During the normalization process, the radiance data obtained from the camera were converted to normalized reflectance (floating point, 32 bit) values between 0 and 100% using the equations below.

$$L_i(\mathbf{x}, \mathbf{y}, \lambda) = \frac{L_r(\mathbf{x}, \mathbf{y}, \lambda)}{R(\mathbf{x}, \mathbf{y}, \lambda)}, \quad (1)$$

$$R(\mathbf{x}, \mathbf{y}, \lambda) = \frac{L_r(\mathbf{x}, \mathbf{y}, \lambda)}{L_i(\mathbf{x}, \mathbf{y}, \lambda)}. \quad (2)$$

The reflectance of the wavelength λ at position x, y is indicated as $R(x, y, \lambda)$, while the incident and reflected lights for the wavelength λ at x, y are denoted as $L_i(x, y, \lambda)$ and $L_r(x, y, \lambda)$, respectively. Using the known reflectance of the reference target and reflected light intensities (radiance) obtained from the HSI camera, Equation 1 will be utilized to estimate incident light across the field of view. Since the HSI camera is a line scanner, we can use Equation 2 to calculate the reflectance of the entire HSI image using the incident light calculated.⁴⁰

3 | METHODOLOGY

SSM uses a reference vector for each class to classify the whole HSI data. The reference spectra are collected from the data set as a mean spectrum for each paper type (Figure 1: Paper1 to Paper40, starting from the top left corner), generating 40 spectral classes from the whole paper data. Here, it is calculated from the HSI data by averaging the 25 spectra from each paper type. The target or test spectra from 40 paper samples are compared with these reference spectra using hybrid SSM to determine their classification capability. The test spectra are generated by randomly selecting approximately 100 pixels from each sample paper, and the results are evaluated based on the confusion matrices. This paper compares eight hybrid SSM to identify the best hybrid measure for the forensic paper classification. The hybrid SSM used here are SID-SAM, SID-SCA, SID-CBD, SID-EUD, CHI-SAM, CHI-SCM, JMD-CHI, and SID-CHI.

3.1 | Individual/original spectral similarity measures

In statistics, similarity measure quantifies the similarity between two data vectors, whereas SSM calculates similarity or dissimilarity between two spectral signatures for imaging spectroscopy. Mainly, it integrates shape (direction of pixel vector) and amplitude (magnitude of pixel vector) features of the spectral signature. If a spectrum is modeled as a vector, it is necessary to consider both the magnitude and the direction.^{41,42} The parameter direction relates to the shape details of each diagnostic feature present in the spectrum. The magnitude expresses the reflectance of the pixel in the spectral dimension. The classifiers SAM, SCA, SID, and JMD are based on shape features.^{23,43} The EUD, CBD, and CHI are distance-based methods based on amplitude features.⁴⁴ As per the parameters considered for matching, the methods can also be classified as deterministic (EUD, CBD, SAM, CHI, and SCA) and stochastic (SID and JMD). Deterministic algorithms depend on the geometrical and physical aspects of the unknown and reference spectra, whereas stochastic algorithms rely on the distributions of the spectral reflectance of target pixels.^{45,46}

3.1.1 | Pixel notations on hyperspectral images

For each HSI data of the paper samples acquired at a particular wavelength λ_i , the pixel vector is represented as $\mathbf{r} = (r_1, r_2, r_3, \dots, r_N)$ where each component r_i represents a pixel in band image B_i and N is the size of the image (width \times height). The corresponding spectral signature of r is defined as $\mathbf{s} = (s_1, s_2, s_3, \dots, s_L)$ where s_i represents the spectral signature of r_i in the form of either radiance or reflectance values, and L is the total number of bands.^{19,28}

3.1.2 | Spectral angle mapper

The SAM is a widely used spectral similarity measure in hyperspectral remote sensing. SAM utilizes the direction of pixel vector, that is, the shape of the spectral signature and treating them as vectors in a spectral space.¹⁴ It calculates

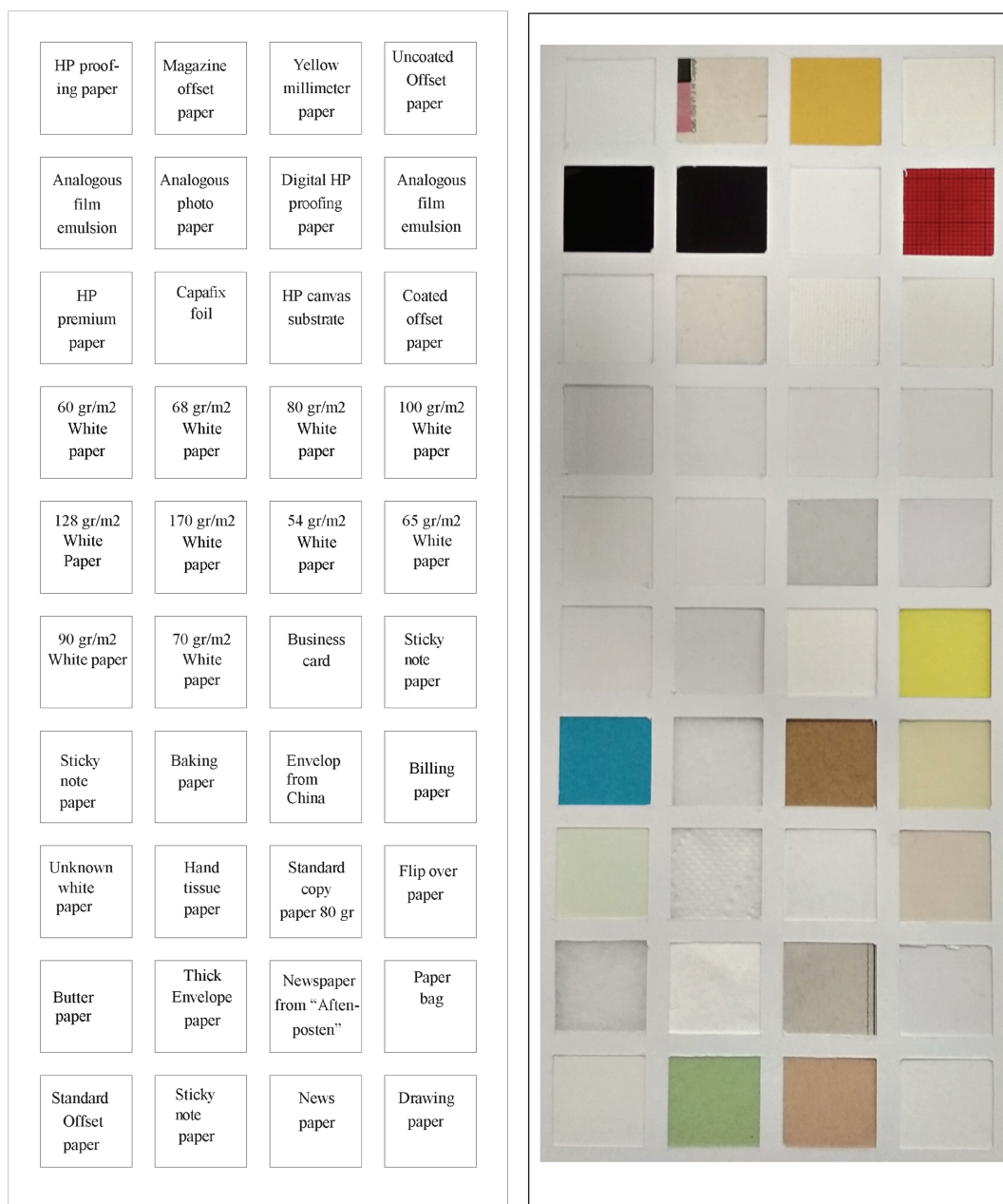


FIGURE 1 Paper checker layout and corresponding paper details³⁹

spectral similarity by measuring the angle between the spectral signatures s_i and s_j corresponding to the pixels r_i and r_j , respectively. The SAM between two spectral signatures s_i and s_j is defined as⁴⁷

$$\text{SAM}(s_i, s_j) = \arccos(s_i \cdot s_j / \|s_i\| \|s_j\|) = \arccos \left(\frac{\left(\sum_{l=1}^L s_{il} s_{jl} \right)}{\sqrt{\sum_{l=1}^L s_{il}^2} \sqrt{\sum_{l=1}^L s_{jl}^2}} \right). \quad (3)$$

This technique is relatively insensitive to unknown and variable illumination, leading to incorrectly matching a poorly illuminated target pixel.

3.1.3 | Spectral correlation mapper

Spectral correlation mapper (SCM) algorithm computes the matching between the spectral vectors based on the parameter “correlation,” where the data are normalized and centered on the mean of the two spectra.^{18,27,48} Correlation measures the strengths of association between two spectra to capture the spectral shape by following the entire length of the spectrum vector.⁴² SCM is derived from Pearsonian correlation coefficient that normalizes and centers the coefficient measure on the average of the target and reference spectra.

The SCM for the two spectral signatures $s_i = (s_{i1}, \dots, s_{iL})^T$ and $s_j = (s_{j1}, \dots, s_{jL})^T$ is shown as

$$\text{SCM}(s_i, s_j) = \frac{\sum_{l=1}^L (s_{il} - \bar{s}_{il})(s_{jl} - \bar{s}_{jl})}{\sqrt{\sum_{l=1}^L (s_{il} - \bar{s}_{il})^2 \sum_{l=1}^L (s_{jl} - \bar{s}_{jl})^2}} \quad (4)$$

For comparison, the coefficient is converted into an angle with the following equation 5.⁴⁹

3.1.4 | The spectral correlation angle

$$\text{SCA}(s_i, s_j) = \arccos\left(\frac{\text{SCM}(s_i, s_j) + 1}{2}\right) \quad (5)$$

The SCA eliminates the negative correlation and maintains the SAM characteristics of minimizing the shading effect.

3.1.5 | Spectral information divergence

The SID is a measure derived from the spectral information measure (SIM)^{19,28} that models the spectral band-to-band variability as a result of uncertainty caused by randomness. The SID utilizes the divergence theory and calculates the probabilistic behaviors between spectral signatures.²⁶ The SID calculates the probabilistic vectors $\mathbf{p} = \{p_l\}_{l=1}^L = (p_1, p_2, p_3, \dots, p_L)^T$ and $\mathbf{q} = \{q_l\}_{l=1}^L = (q_1, q_2, q_3, \dots, q_L)^T$ for the spectral signatures of two-pixel vectors, s_i and s_j ^{19,43} where $p_k = \frac{s_{ik}}{\sum_{l=1}^L s_{il}}$ and $q_k = \frac{s_{jk}}{\sum_{l=1}^L s_{jl}}$.⁵⁰

SID between two pixels r_i and r_j is expressed as follows:

$$\text{SID}(r_i, r_j) = D(r_i \| r_j) + D(r_j \| r_i), \quad (6)$$

where the relative entropy of r_j with respect to r_i is

$$D(r_i \| r_j) = \sum_{l=1}^L p_l \log\left(\frac{p_l}{q_l}\right), \quad (7)$$

and the relative entropy of r_i with respect to r_j is,

$$D(r_j \| r_i) = \sum_{l=1}^L q_l \log\left(\frac{q_l}{p_l}\right). \quad (8)$$

p_l and q_l are the probability vectors of s_i and s_j , respectively, for the l th band.

3.1.6 | Jeffries–Matusita distance

JMD⁵⁰ computes the separability of the target and reference spectral vectors by allowing band-wise spectral information. The probability density of the unknown target and reference spectral vectors, r_i and r_j for bands is computed as^{20,51,52}

$$\text{JMD}(r_i, r_j) = \sqrt{\sum_{l=1}^L [\sqrt{p_l} - \sqrt{q_l}]^2}, \quad (9)$$

where p_l and q_l are the probability vectors of s_i and s_j , respectively, for the l th band.

3.1.7 | Euclidean distance

EUD measures the ordinary distance between two materials where a smaller EUD value means greater similarity. EUD is sensitive to outliers and offset and gain errors.⁴³ It computes the distance between two spectra s_i and s_j in the n -dimensional spectral feature space, is defined as

$$\text{EUD}(s_i, s_j) = \sqrt{\sum_{l=1}^L (s_{il} - s_{jl})^2}. \quad (10)$$

3.1.8 | City block distance

The CBD, alias Manhattan distance, represents the sum of the absolute differences between two-pixel vectors r_i and r_j or spectral signatures s_i and s_j ,^{53,54} and it is defined as below equation:

$$\text{CBD}(s_i, s_j) = \sum_{l=1}^L |s_{il} - s_{jl}|. \quad (11)$$

3.1.9 | Chi-square distance

CHI is an important measure in image analysis applications²¹; it is a nonparametric classification technique that allows data classification and analysis with no preassumed distribution. It is a nonlinear metric derived from Pearson's chi-squared test statistic,²² and it creates a predictive model that minimizes the misclassifications.³² The CHI²¹ between two spectral signatures $s_i = (s_{i1}, s_{i2}, \dots, s_{il})$ and $s_j = (s_{j1}, s_{j2}, \dots, s_{jl})$ is defined as⁵⁵

$$\text{CHI}(s_i, s_j) = \frac{1}{2} \sum_{l=1}^L \frac{(s_{il} - s_{jl})^2}{(s_{il} + s_{jl})}. \quad (12)$$

3.2 | Conceptualizing hybrid spectral similarity measures

As the hybrid SSM are produced by fusing the spectral capabilities of two or more matching algorithms, they are expected to overcome the limitations in the accuracy of the individual algorithms.^{28,56} They are produced by orthogonally projecting the spectral capabilities of individual measures based on the tangent function. Thus, the combination of stochastic and deterministic techniques could make an optimal hybrid that increases distinguishability by enhancing

the similarity or dissimilarity between spectrums. The following hybrid SSM are used in this work: CHI-SAM, CHI-SCM, JMD-CHI, SID-CBD, SID-CHI, SID-EUD, SID-SAM, and SID-SCA and they can be defined as below equations.

$$\text{CHISAM}_{\tan}(s_i, s_j) = \text{CHI}(s_i, s_j) (\tan(\text{SAM}(s_i, s_j))). \quad (13)$$

In Equation 13, CHI and SAM can be substituted with other similarity measures to achieve the other hybrid SSM.

3.3 | Accuracy assessment

In order to estimate the percentage of correctly classified pixels, a post-classification accuracy assessment is carried out. The confusion matrix is produced to assess the accuracy of all the hybrid SSM where the overall accuracy (OA), kappa (\hat{K}), Z-score of kappa ($Z(\hat{K})$), and the 95% confidence interval of kappa ($\text{CI}(\hat{K})$) are calculated. The overall accuracy denotes the percentage of all validation pixels classified correctly. It is usually expressed as a percent, with 100% accuracy, making a perfect classification where all test spectra are classified correctly. Generally, the value of kappa is normalized between 0 to 1 and is interpreted as ≤ 0 indicates no agreement, 0.01–0.20 none to a slight agreement, 0.21–0.40 fair agreement, 0.41–0.60 moderate agreement, 0.61–0.80 substantial agreement, and 0.81–1.00 almost a perfect agreement. Also, any kappa obtained below 0.60 specifies inadequate agreement among the raters, with no confidence in such study results.^{36,57} The equations of kappa (\hat{K}), kappa variance ($\widehat{\text{Var}}(\hat{K})$), Z-score of kappa ($Z(\hat{K})$), and the 95% confidence interval of kappa ($\text{CI}(\hat{K})$) are written as follows:

$$\text{Kappa, } \hat{K} = \frac{(P_O - P_E)}{(1 - P_E)}, \quad (14)$$

where P_O is the observed agreement and is the same as the OA and P_E is the expected agreement.

$$\text{Variance, } \widehat{\text{Var}}(\hat{K}) = \frac{P_O(1 - P_E)}{N(1 - P_E)^2}, \quad (15)$$

where N is the total number of samples.

$$\text{Z-score of Kappa, } Z(\hat{K}) = \frac{\hat{K}}{\sqrt{\widehat{\text{Var}}(\hat{K})}}. \quad (16)$$

If the kappa variance is found minimum and the Z value obtained is higher than 1.96, the classification results imply better classification at a 95% confidence level. Also, the kappa's confidence interval is determined to get an estimation based on the desired 95% confidence level. Hence, the results produced from this research could well define the multiclass classification ability of the best hybrid SSM for classifying the 40 hyperspectral images of the paper samples.

To streamline the accuracy of the hybrid SSM, it is very much necessary to optimize the performances based on error matrices like mean absolute error (MAE), root mean squared error (RMSE), and R^2 (coefficient of determination). MAE is the average of the sum of the absolute differences between the original and predicted values. RMSE is obtained from the square root of mean squared error, which is the difference between the original and predicted values obtained by squaring the average difference over the data set. Lower values of MAE and RMSE indicate better accuracy, whereas R^2 represents the coefficient of how much better the model is. It measures the amount of variation produced by the hybrid SSM, that is, the percentage of correct predictions. R^2 values can range from 0 to 1. A value of 0 indicates that the response variable cannot be explained by the predictor variable and a value of 1 indicates that the response variable can be flawlessly explained without error by the predictor variable.

4 | RESULTS AND DISCUSSION

The mean reference spectra obtained for all the paper samples are shown in Figure 2. Most of the paper samples produced nearly similar responses in the near-infrared region (NIR) and showed distinct features in the visible region. Also, a spectral peak can be seen near 450 nm, which goes beyond the maximum reflectance value due to the fluorescence emission from the materials. As expected, the darker materials possess a relatively lower reflectance profile in the visible region; however, they showed a slight increase toward the NIR range.

The hybrid SSM, namely, CHI-SAM, CHI-SCM, JMD-CHI, SID-CBD, SID-CHI, SID-EUD, SID-SAM, and SID-SCA, are evaluated using HSI paper data, and they are implemented using Matlab 2021a. Their classification capabilities are evaluated using indexes obtained from the confusion matrix (Supporting Information). Here, SID-CBD and SID-EUD failed to produce valid confusion matrices, so their classification results could not be considered in this study. The remaining resultant classified images of the six hybrid SSM, namely, CHI-SAM, CHI-SCM, JMD-CHI, SID-CHI, SID-SAM, and SID-SCA, can be seen in Figure 3.

It is noticeable in Figure 3 that paper 31 (standard copy paper 80 g) overlaps more into other classes, most predominantly found in the classification done by CHI-SAM, CHI-SCM, SID-CHI, and JMD-CHI. The OA obtained for various SSM are mentioned in Table 1 below.

From Figure 3, it is clear that Paper 3 (yellow millimeter paper), Paper 5 (analogous film emulsion), Paper 6 (analogous photo paper), Paper 20 (65 g/m² white paper), Paper 24 (sticky note paper), Paper 25 (sticky note paper), Paper 27 (envelop from china), Paper 28 (billing paper), Paper 29 (unknown white paper), Paper 38 (sticky note paper), and Paper 39 (newspaper) are perfectly classified by all the hybrid SSM. In contrast, Paper 9 (HP premium paper), Paper 13 (60 g/m² white paper), Paper 21 (90 g/m² white paper), Paper 26 (baking paper), and Paper 33 (butter paper) was almost entirely misclassified by all the hybrid SSM. We analyzed the overall accuracy (OA) of the hybrid SSM where the SID-SCA achieved the highest accuracy of 88%, followed by SID-SAM with 87%. The measures SID-CHI, JMD-CHI, CHI-SAM, and CHI-SCM, produced OA of 80%, 72%, 72%, and 71%, respectively. These results can be attributed to their proven capabilities for capturing high band-to-band variability for hyperspectral images that measure the similarity between two pixel vectors.⁴⁴ The hybrid combination SID-SCA is mainly dependent on the shape of the curve, not by the amplitude values of reflectance curves. This affirms that the individual measures SID and SCA, which consider only

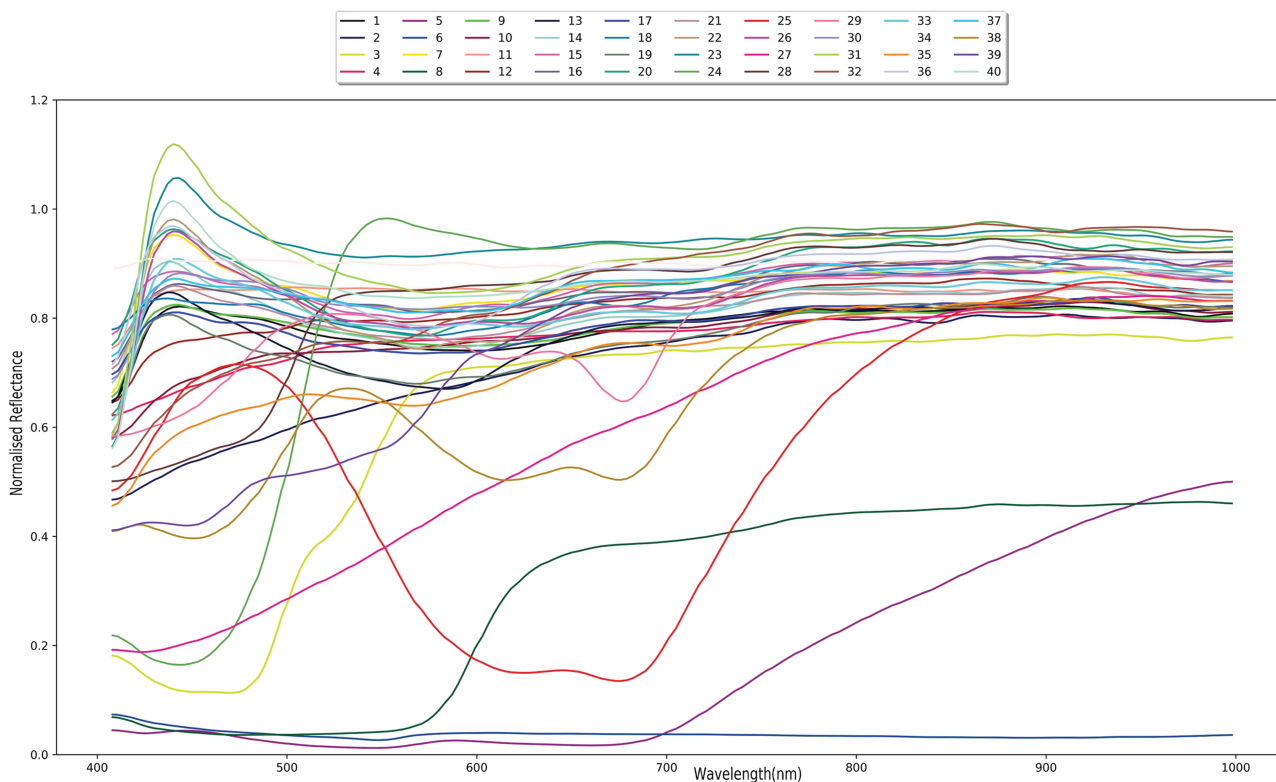


FIGURE 2 Mean spectra of papers used³⁹

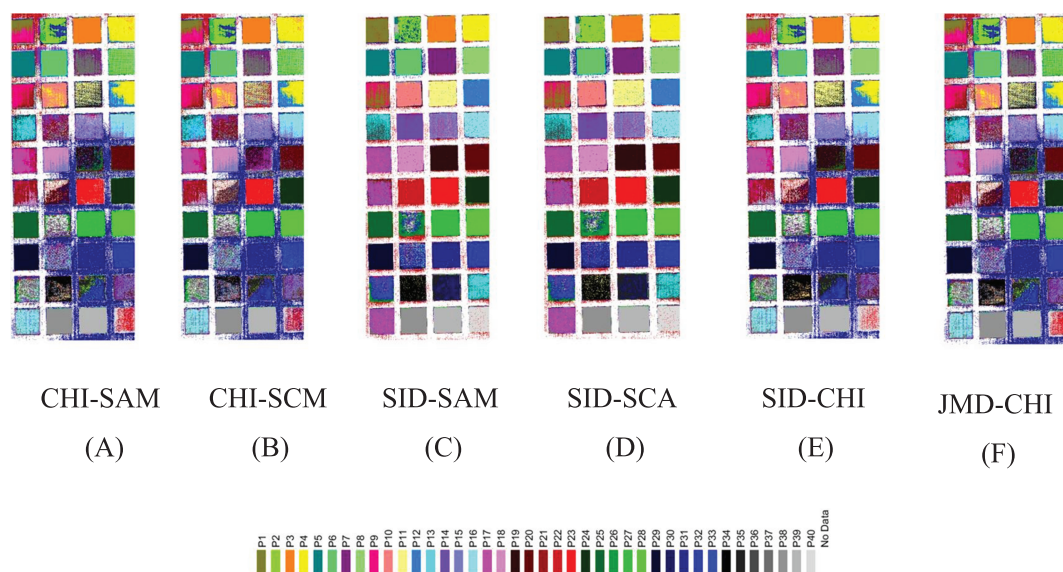


FIGURE 3 Classification results of paper samples

TABLE 1 The overall accuracy (OA) of hybrid SSM

SSM	CHI-SAM	CHI-SCM	SID-SAM	SID-SCA	SID-CHI	JMD-CHI
OA	71%	71%	87%	88%	80%	72%

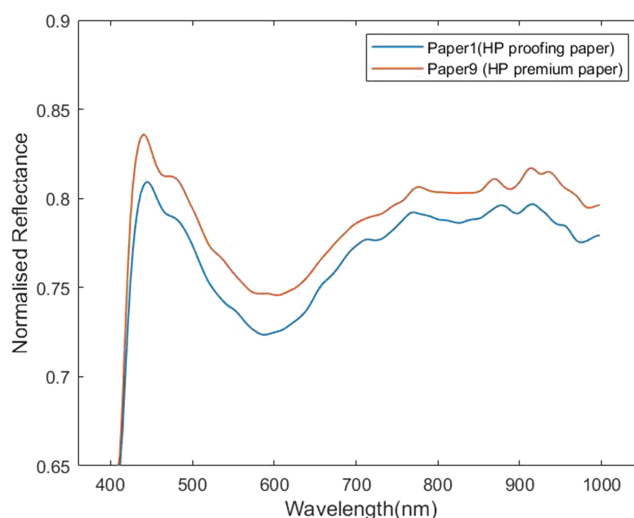


FIGURE 4 Reflectance curves for paper 1 and paper 9

the shape of the curve. This can be exemplified from the classified images of SID-SCA in Figure 4. In this case, Paper 9 (HP premium paper) is misclassified as paper 1 (HP proofing paper), showing a similar shape for the reflectance curves for these papers but with varying amplitude.

Also, checked paper 21 (90 g/m² white paper), which has misclassified pixels prevalently from paper 17 (128 g/m² white paper), showed their spectra as in Figure 5. Here also, the reflectance curves can be seen with similar shapes with varying amplitude.

The kappa, MAE, RMSE, R^2 , and related parameters for each hybrid SSM are also evaluated to validate the results based on OA. The results are provided in Table 2 below. In addition to the kappa score, the confidence interval of

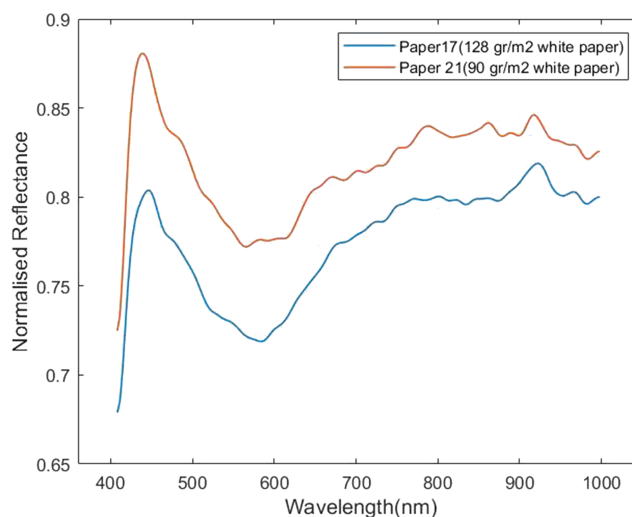


FIGURE 5 Reflectance curves for Paper 17 and Paper 21

TABLE 2 Different evaluation factors used and its corresponding results for each hybrid method

Methods	Kappa	CI of kappa@95%	Z-score of kappa	MAE	RMSE	R^2
SID-SCA	0.88	0.87-0.89	168.72	0.12	2.32	0.95
SID-SAM	0.87	0.86-0.89	163.66	0.13	2.35	0.95
SID-CHI	0.8	0.79-0.81	125.73	0.20	3.41	0.89
JMD-CHI	0.71	0.70-0.72	98.59	0.28	4.42	0.81
CHI-SAM	0.71	0.70-0.72	98.89	0.28	4.41	0.81
CHI-SCM	0.71	0.69-0.72	97.63	0.29	4.43	0.81

kappa@95% and Z-score of kappa are calculated for the different hybrid SSM. Here, higher values indicate better discrimination capabilities.

The kappa coefficient is a statistical measurement generally used to assess the accuracy of confusion matrices by measuring how well the classified data agrees with the reference data. The hybrid measure SID-SCA obtained the highest kappa value of 0.88, and SID-SAM obtained 0.87 produced a nearly perfect agreement, which implies that the reference data are appropriately classified. However, SID-CHI, JMD-CHI, CHI-SAM, and CHI-SCM obtained lower values, demonstrating substantial agreement, indicating that the reference data are classified not to the best. Thus, it is proved that SID-SCA is effective in classifying the 40 hyperspectral paper samples. Then, for the Z-score values again, SID-SCA (168.72) obtained a higher value of 168.72, followed by SID-SAM, SID-CHI, JMD-CHI, CHI-SAM, and CHI-SCM. The prediction error matrix MAE obtained lower values of 0.12 and 0.13 for SID-SCA and SID-SAM, respectively. The RMSE, the SID-SCA and SID-SAM have obtained lower values of 2.32 and 2.35, respectively. The R^2 has the highest values of 0.95 for both SID-SCA and SID-SAM, demonstrating that the response variable can be perfectly explained without error by the predictor variable. Thus, the kappa values, MAE, RMSE, and R^2 validated the results of overall accuracy by selecting SID-SCA as the best hybrid SSM for hyperspectral paper sample classification. The results from this study enable forensic researchers to make the correct choice of classification algorithm for hyperspectral data analysis of similar materials.

5 | CONCLUSION

This research presented the classification efficiency of eight hybrid spectral similarity algorithms to classify hyperspectral paper data. Hybrid spectral similarity measures are rarely applied in forensic research. The efficacy of these

measures on close-range hyperspectral data analysis is presented in this paper. The SID-CBD and SID-EUD failed to produce valid confusion matrices; the remaining six hybrid spectral similarity measures, namely, CHI-SAM, CHI-SCM, JMD-CHI, SID-CHI, SID-SAM, and SID-SCA, are evaluated for their classification capability. Analyzing the statistics of the results obtained, it is found that SID-SCA produced the highest overall accuracy of 88%, which is justifiable in forensic applications.^{58,59} From the validation based on kappa, confidence interval of kappa@95%, Z-score of kappa, MAE, RMSE, and R^2 , the SID-SCA can be considered as the best hybrid measure with a perfect agreement for kappa. Thus, from this study based on spectral similarity statistics, the enhanced accuracy of SID-SCA for the classification of hyperspectral paper data is achieved, thereby underlining the importance of spectral similarity analysis on close-range hyperspectral image data.

PEER REVIEW

The peer review history for this article is available at <https://publons.com/publon/10.1002/cem.3387>.

DATA AVAILABILITY STATEMENT

Data will be provided on request.

ORCID

Binu Melit Devassy  <https://orcid.org/0000-0003-1860-9749>

Sony George  <https://orcid.org/0000-0001-8436-3164>

REFERENCES

1. Jones K, Benson S, Roux C. The forensic analysis of office paper using carbon isotope ratio mass spectrometry. Part 3: characterizing the source materials and the effect of production and usage on the $\delta^{13}\text{C}$ values of paper. *Forensic Sci Int*. 2013;233(1-3):355-364. doi: 10.1016/j.forsciint.2013.10.011
2. Chesson LA, Tipple BJ, Barnette JE, Cerling TE, Ehleringer JR. The potential for application of ink stable isotope analysis in questioned document examination. *Sci Justice*. 2015;55(1):27-33. doi:10.1016/j.scijus.2014.05.010
3. Zlotnick JA, Smith FP. Chromatographic and electrophoretic approaches in ink analysis. *J Chromatogr B Biomed Sci Appl*. 1999; 733(1-2):265-272. doi:10.1016/S0378-4347(99)00312-6
4. Corregidor V, Viegas R, Ferreira LM, Alves LC. Study of iron gall inks, ingredients and paper composition using non-destructive techniques. *Heritage*. 2019;2(4):2691-2703. doi:10.3390/heritage2040166
5. Khan MJ, Khan HS, Yousaf A, Khurshid K, Abbas A. Modern trends in hyperspectral image analysis: a review. *IEEE Access*. 2018;6: 14118-14129. doi:10.1109/ACCESS.2018.2812999
6. Deborah H, George S, Hardeberg JY. Spectral-divergence based pigment discrimination and mapping: a case study on The Scream (1893) by Edvard Munch. *J Am Inst Conserv*. 2019;58(1-2):90-107. doi:10.1080/01971360.2018.1560756
7. Lu G, Fei B. Medical hyperspectral imaging: a review. *J Biomed Opt*. 2014;19(1):010901. doi:10.1117/1.jbo.19.1.010901
8. Melit Devassy B, George S. Contactless classification of strawberry using hyperspectral imaging. In CEUR Workshop Proceedings, 2020, vol. 2688. <https://ntnuopen.ntnu.no/ntnu-xmlui/handle/11250/2727296>
9. Melit Devassy B, George S. Forensic analysis of beverage stains using hyperspectral imaging. *Sci Rep*. 2021;11(1):1-13. doi: 10.1038/s41598-021-85737-x
10. Manolakis DG, Shaw G. Detection algorithms for hyperspectral imaging applications. *IEEE Signal Process Mag*. 2002;19(1):29-43. doi: 10.1109/79.974724
11. Song A, Choi J, Kim Y, Kim Y. Analysis of appropriate spectral similarity methods to classify target species using CASI hyperspectral images, ACRS 2015-36th Asian Conf. Remote Sens. Foster. Resilient Growth Asia, Proc, 2015.
12. Manolakis D, Lockwood R, Cooley T, Jacobson J. Is there a best hyperspectral detection algorithm? *Algorithms Technol Multispectral, Hyperspectral, Ultraspectral Imag XV*. 2009;7334:733402. doi:10.1117/12.816917
13. Chauhan H, Krishna Mohan B. Effectiveness of spectral similarity measures to develop precise crop spectra for hyperspectral data analysis. *ISPRS Ann Photogramm Remote Sens Spat Inf Sci*. 2014;II-8, no. December:83-90. doi:10.5194/isprsannals-II-8-83-2014
14. Kruse FA, Lefkoff AB, Boardman JW, et al. The spectral image processing system (SIPS)—interactive visualization and analysis of imaging spectrometer data. *Remote Sens Environ*. 1993;44(2):145-163. doi:10.1016/0034-4257(93)90013-N
15. Girouard G, Bannari A. Validated spectral angle mapper algorithm for geological mapping: comparative study between QuickBird and Landsat-TM, XXth ISPRS Congr.; 2004: 599-604.
16. Swain MJ, Ballard DH. Color indexing. *Int J Comput Vis*. 1991;7(1):11-32. doi:10.1007/BF00130487
17. Granahan JC, Sweet JN. An evaluation of atmospheric correction techniques using the spectral similarity scale. In: *IGARSS 2001. Scanning the Present and Resolving the Future. Proceedings. IEEE 2001 International Geoscience and Remote Sensing Symposium (Cat. No. 01CH37217)*, Vol. 5. IEEE; 2001:2022-2024.

18. de Carvalho OA Jr, Meneses PR. Spectral correlation mapper (SCM): an improvement on the spectral angle mapper (SAM). In: *Summaries of the 9th JPL Airborne Earth Science Workshop, JPL Publication 00-18*. JPL Publication; 2000.
19. Chang CI. An information-theoretic approach to spectral variability, similarity, and discrimination for hyperspectral image analysis. *IEEE Trans Inf Theory*. 2000;46(5):1927-1932. doi:10.1109/18.857802
20. Bruzzone L, Roli F, Serpico SB. An extension of the Jeffreys–Matusita distance to multiclass cases for feature selection. *IEEE Trans Geosci Remote Sens*. 1995;33(6):1318-1321. doi:10.1109/36.477187
21. Ren H, Xiao S, Zhou H. A chi-square distance-based similarity measure of single-valued neutrosophic set and applications. *Int J Comput Commun Control*. 2019;14(1):78-89. doi:10.15837/ijccc.2019.1.3430
22. Yang W, Xu L, Chen X, Zheng F, Liu Y. Chi-squared distance metric learning for histogram data. *Math Probl Eng*. 2015;2015:352849. doi:10.1155/2015/352849
23. Kumar MN, Seshasai MV, Prasad KV, et al. A new hybrid spectral similarity measure for discrimination among vigna species. *Int J Remote Sens*. 2011;32(14):4041-4053. doi:10.1080/01431161.2010.484431
24. Li Q, Niu C. Feature-enhanced spectral similarity measure for the analysis of hyperspectral imagery. *J Appl Remote Sens*. 2015;9(1):096008. doi:10.1117/1.jrs.9.096008
25. Thomas T, Deepthi. Performance comparison of hyperspectral oil spill detection algorithms using hybrid similarity measures, Proc. IDES Jt. Int. Conf. Adv. Signal Process. Commun. – SPC 2018, 2018.
26. Chang CI, Spectral information divergence for hyperspectral image analysis, in *International Geoscience and Remote Sensing Symposium (IGARSS)*. IEEE; 1999. doi:10.1109/igarss.1999.773549
27. van der Meer F. The effectiveness of spectral similarity measures for the analysis of hyperspectral imagery. *Int J Appl Earth Obs Geoinf*. 2006;8(1):3-17. doi:10.1016/j.jag.2005.06.001
28. Chang CI. New hyperspectral discrimination measure for spectral characterization. *Opt Eng*. 2004;43(8):1777. doi:10.1117/1.1766301
29. Deepthi, Thomas T. Spectral similarity algorithm-based image classification for oil spill mapping of hyperspectral datasets. *J Spectr Imaging*. 2020;9(a14):1-17. doi:10.1255/jsi.2020.a14
30. Weih RC, Riggan ND. Object-based classification vs. pixel-based classification: comparative importance of multi-resolution imagery. *Int Arch Photogramm Remote Sens Spat Inf Sci*. 2010;XXXVIII:1-6.
31. Lamine S, Petropoulos GP, Singh SK, et al. Quantifying land use/land cover spatio-temporal landscape pattern dynamics from Hyperion using SVMs classifier and FRAGSTATS®. *Geocarto Int*. 2018;33(8):862-878. doi:10.1080/10106049.2017.1307460
32. Shahi K, Shafri HZM, Hamedianfar A. Road condition assessment by OBIA and feature selection techniques using very high-resolution WorldView-2 imagery. *Geocarto Int*. 2017;32(12):1389-1406. doi:10.1080/10106049.2016.1213888
33. Petropoulos GP, Vadrevu KP, Kalaitzidis C. Spectral angle mapper and object-based classification combined with hyperspectral remote sensing imagery for obtaining land use/cover mapping in a Mediterranean region. *Geocarto Int*. 2013;28(2):114-129. doi:10.1080/10106049.2012.668950
34. Myint SW, Mesev V, Quattrochi DA, Wentz EA. Urban image classification: per-pixel classifiers, subpixel analysis, object-based image analysis, and geospatial methods. *Remote Sens Data Charact Classif Accuracies*. 2015;1:219-230. doi:10.1201/b19294
35. Rwanga SS, Ndambuki JM. Accuracy assessment of land use/land cover classification using remote sensing and GIS. *International Journal of Geosciences*. 2017;08(04):611-622. doi:10.4236/ijg.2017.84033
36. Viera AJ, Garrett JM. Understanding interobserver agreement: the kappa statistic. *Fam Med*. 2005;37(5):360-363.
37. Congalton RG, Green K. Basic analysis techniques, *Assess. Accuracy Remote. Sensed Data*. CRC Press; 2009: 127-144. doi:10.1201/9780429052729-8
38. Hazra A, Using the confidence interval confidently, *J Thorac Dis*, vol. 9, no. 10, pp. 4124-4129, Oct. 2017. doi:10.21037/jtd.2017.09.14
39. Melit Devassy B, George S, Nussbaum P. Unsupervised clustering of hyperspectral paper data using t-SNE. *J Imaging*. 2020;6(5):29. doi:10.3390/jimaging6050029
40. Devassy B, George S. Estimation of strawberry firmness using hyperspectral imaging: a comparison of regression models. *J Spectr Imaging*. 2021. doi:10.1255/jsi.2021.a3
41. Granahan JC, Sweet JN. An evaluation of atmospheric correction techniques using the spectral similarity scale, *IGARSS 2001. Scanning Present Resolv. Futur. Proceedings. IEEE 2001 Int. Geosci. Remote Sens. Symp. (Cat. No.01CH37217)*, vol. 5, no. C, pp. 7031–7033, 2001. doi:10.1109/IGARSS.2001.977890
42. Padma S, Sanjeevi S. Spectral correlation and Jeffreys–Matusita based matching algorithm for improved Information extraction from hyperspectral images, Proc 37th Asian Conf Remote Sens, 2016.
43. Song A, Choi J, Kim Y, Kim Y. Analysis of appropriate spectral similarity methods to classify target species using CASI hyperspectral images, *ACRS 2015-36th Asian Conf. Remote Sens. Foster. Resilient Growth Asia, Proc.*, vol. 1, no. 1, 2015.
44. Sharma S, Role of Hybrid Spectral Similarity Measures for Semi-Supervised Fuzzy Classifier, Enschede, 2018. <https://www.iirs.gov.in/content/role-hybrid-spectral-similarity-measures-semi-supervised-fuzzy-classifier>
45. Shanmugam S, Srinivasa Perumal P. Spectral matching approaches in hyperspectral image processing. *Int J Remote Sens*. 2014;35(24):8217-8251. doi:10.1080/01431161.2014.980922
46. Homayouni S, Roux M. Hyperspectral image analysis for material mapping using spectral matching. In: *Int. Arch. Photogramm. Remote Sens. Spat. Inf. Sci. - ISPRS Arch*. Vol. 35; 2004.
47. Yuhas RH, Goetz AF, Boardman JW. Discrimination among semi-arid landscape endmembers. In: *JPL, Summaries of the Third Annual JPL Airborne Geoscience Workshop*; 1992:147-149.

48. Shivakumar BR, Rajashekararadhya SV. Performance evaluation of spectral angle mapper and spectral correlation mapper classifiers over multiple remote sensor data, *Proc. 2017 2nd IEEE Int. Conf. Electr. Comput. Commun. Technol. ICECCT 2017*. IEEE; 2017:1-6. doi:10.1109/ICECCT.2017.8117946
49. Robila S, Hall R, Montclair U. An investigation of spectral metrics in hyperspectral image preprocessing for classification. In: *Geospatial Goes Global: From Your Neighborhood to the Whole Planet*. ASPRS; 2005:7-11.
50. Ghiyamat A, Shafri HZM, Mahdiraji GA, Shariff ARM, Mansor S. Hyperspectral discrimination of tree species with different classifications using single- and multiple-endmember. *Int J Appl Earth Obs Geoinf*. 2013;23:177-191. doi:10.1016/j.jag.2013.01.004
51. Swain PH, King RC. Two effective feature selection criteria for multispectral remote sensing, LARS Tech Reports, pp. 536-540, 1973.
52. Toussaint GT. Some inequalities between distance measures for feature evaluation. *IEEE Trans Comput*. 1972;C-21(4):409-410. doi:10.1109/TC.1972.5008991
53. Chang C-I. *Hyperspectral Imaging: Techniques for Spectral Detection and Classification*. Norwell: Kluwer Academic; 2003.
54. Perlibakas V. Distance measures for PCA-based face recognition. *Pattern Recognit Lett*. 2004;25(6):711-724. doi:10.1016/j.patrec.2004.01.011
55. Pele O, Werman M. The quadratic-chi histogram distance family. In: Daniilidis K, Maragos P, Paragios N, eds. *Computer Vision—ECCV 2010*. Vol. 2010. Springer Berlin Heidelberg; 749-762.
56. Vishnu S, Nidamanuri RR, Bremananth R. Spectral material mapping using hyperspectral imagery: a review of spectral matching and library search methods. *Geocarto Int*. 2013;28(2):171-190. doi:10.1080/10106049.2012.665498
57. Landis JR, Koch GG. The measurement of observer agreement for categorical data, *Biometrics*, vol. 33, no. 1, p. 159, 1977. doi:10.2307/2529310
58. Zhang Q, Liu Y, Wang F, Lu J, Li D, Fusion CNN based on feature selection for crime scene investigation image classification, in *Advances in Intelligent Systems and Computing*, vol 1075. Springer; 2020. doi:10.1007/978-3-030-32591-6_83
59. Liu Y, Attinger D, De Brabanter K. Automatic classification of bloodstain patterns caused by gunshot and blunt impact at various distances. *J Forensic Sci*. 2020;65(3):729-743. doi:10.1111/1556-4029.14262

SUPPORTING INFORMATION

Additional supporting information may be found in the online version of the article at the publisher's website.

How to cite this article: Deepthi, Devassy BM, George S, Nussbaum P, Thomas T. Classification of forensic hyperspectral paper data using hybrid spectral similarity algorithms. *Journal of Chemometrics*. 2022;36(1):e3387. doi:10.1002/cem.3387